Hemodynamic Analysis of Growing Intracranial Aneurysms Arising from a Posterior Inferior Cerebellar Artery

Shin-Ichiro Sugiyama[1], Hui Meng[3,4], Kenichi Funamoto[4], Takashi Inoue[2], Miki Fujimura[2], Toshio Nakayama[4], Shunsuke Omodaka[5], Hiroaki Shimizu[2], Akira Takahashi[6], Teiji Tominaga[5]

Key words
- Hemodynamics
- Intracranial aneurysm
- Wall shear stress

Abbreviations and Acronyms
3D: Three-dimensional
CFD: Computational fluid dynamics
MR: Magnetic resonance
OSI: Oscillatory shear index
PICA: Posterior inferior cerebellar artery
VA: Vertebral artery
WSS: Wall shear stress

From the Departments of [1]Neuroanesthesia and [2]Neurosurgery, Kohnan Hospital, Sendai, Japan; [3]Toshiba Stroke Research Center, University at Buffalo, The State University of New York, Buffalo, New York, USA; [4]Institute of Fluid Science, Tohoku University, Sendai, Japan; and Departments of [5]Neurosurgery and [6]Neuroendovascular Therapy, Tohoku University Graduate School of Medicine, Sendai, Japan

To whom correspondence should be addressed: Shin-ichiro Sugiyama, M.D., Ph.D. [E-mail: sushi@kohnan-sendai.or.jp]

Citation: World Neurosurg. (2012) 78, 5:462-468.
DOI: 10.1016/j.wneu.2011.09.023

*Journal homepage: **www.WORLDNEUROSURGERY.org***

*Available online: **www.sciencedirect.com***

1878-8750/$ - see front matter

OBJECTIVE: **The role of hemodynamics in the growth of intracranial aneurysms is not completely clear. We present a hemodynamic study with two adjacent unruptured aneurysms arising from one parent artery but growing in different ways. This study aimed to investigate whether there were differences in hemodynamic characteristics between the two growing aneurysms.**

METHODS: **A 62-year-old female patient presented with six unruptured intracranial aneurysms. Catheter angiography at 6-month intervals revealed that two aneurysms located adjacently at the right posterior inferior cerebellar artery were growing over a 1-year period. Three-dimensional aneurysm geometries were acquired via rotational angiography. Computational fluid dynamic simulations were conducted on the 3D aneurysm geometries under patient-specific pulsatile flow conditions that were measured by magnetic resonance velocimetry.**

RESULTS: **The proximal multilobular aneurysm demonstrated high flow and physiological levels of wall shear stress (WSS) in the region of growth, whereas the distal rounded aneurysm had low flow and low WSS in the growing sac.**

CONCLUSION: **Growing aneurysms can have heterogeneous hemodynamic and morphologic characteristics and different growing patterns. Growing regions of an aneurysm could be exposed to either high WSS at the inflow zone or low WSS and high oscillatory shear in the aneurysm sac.**

INTRODUCTION

Hemodynamics is thought to influence the initiation, growth, and rupture of intracranial aneurysms (16). Although there seems to be general consensus that high wall shear stress (WSS) results in the initiation of intracranial aneurysms (13-16), the hemodynamic conditions that drive the growth of aneurysms after initiation are still not completely clear. High WSS has been postulated to account for aneurysm progression from the distal neck where flow impinges (6, 8), whereas low WSS has been associated with aneurysm growth in the dome (1, 18, 19).

We present a hemodynamic study of two adjacent aneurysms originating from one parent artery but growing in different ways. Longitudinal data sets of 3D rotational angiography were used to reconstruct accurate geometries of the aneurysms and adjacent arteries. The purpose of this study was to determine whether there were differences in the hemodynamic characteristics of the two growing aneurysms.

MATERIALS AND METHODS

Case Presentation

A 62-year-old hypertensive female patient presented with vertigo. Computed tomographic imaging showed no evidence of hemorrhage but the presence of multiple intracranial aneurysms. Magnetic resonance (MR) angiography performed in April 2009 revealed six intracranial aneurysms: two in the right middle cerebral artery, two adjacent ones in the right posterior inferior cerebellar artery (PICA), one in the left middle cerebral artery, and one at the tip of the basilar artery (**Figure 1**). The two right middle cerebral artery aneurysms were clipped in May 2009, and the basilar tip aneurysm was treated via coil embolization in August 2009. The presurgical angiographic data were inaccessible digitally because of the unfortunate failure of a data storage device. The angiograph acquired during the coiling was therefore defined as the baseline for computational fluid dynamic (CFD) analysis. Thereafter, the patient's progress was followed up by angiography at 6-month intervals (first follow-up in February 2010; second follow-up in August 2010).

Between the initial angiograph and that obtained during embolization of the basilar tip aneurysm, the three untreated aneurysms showed no detectable change in shape or size. However, the two follow-up angiographs revealed that the two aneurysms in the right PICA had grown over time (**Figure 2**). The proximal multilobular aneu-

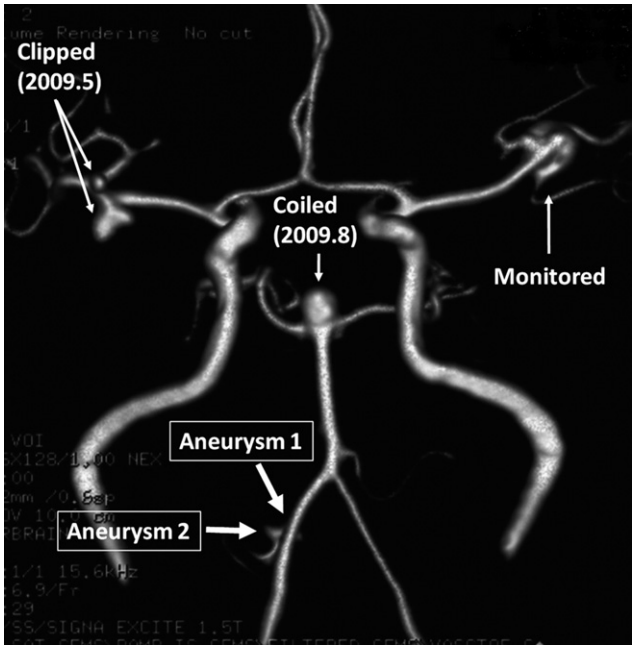

Figure 1. Magnetic resonance angiography at the initial presentation in April 2009 showing six aneurysms in this patient: two in the right middle cerebral artery, which were clipped in May 2009; one at the tip of the basilar artery, which was coiled in August 2009; and one in the left middle cerebral artery and two in the right posterior inferior cerebellar artery (PICA), referred to as Aneurysm 1 and Aneurysm 2.

rysm at the PICA–vertebral artery (VA) junction (Aneurysm 1) showed partial enlargement of the aneurysm wall, whereas the distal, more spherical aneurysm (Aneurysm 2) showed enlargement of the whole aneurysm body.

One month after the last angiography, the two growing PICA aneurysms were clipped individually via open occipital craniotomy. Aneurysm 1 had yellow blebs with atherosclerosis, whereas Aneurysm 2 was reddish and thin walled (**Figure 3**).

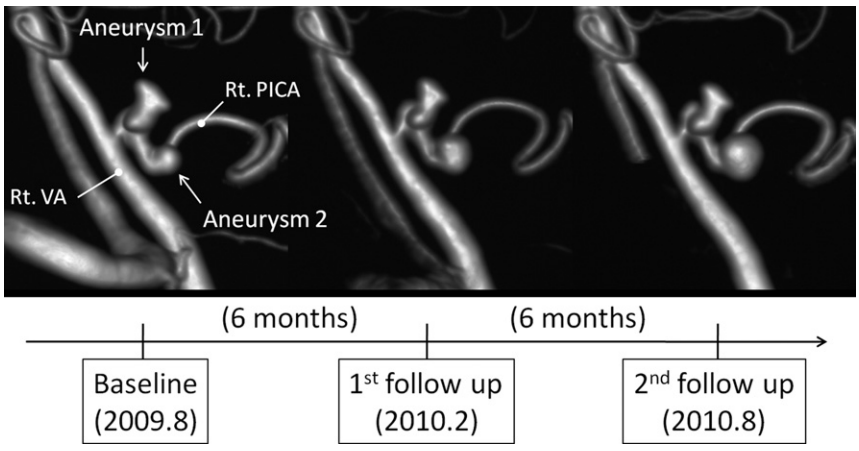

Figure 2. Three-dimensional rotational digital angiography of the two PICA aneurysms at three time points: baseline (August 2009), first follow-up (February 2010), and second follow-up (August 2010), showing that they grew over time. Both aneurysms were subsequently clipped in September 2010. PICA, posterior inferior cerebellar artery; Rt., right; VA, vertebral artery.

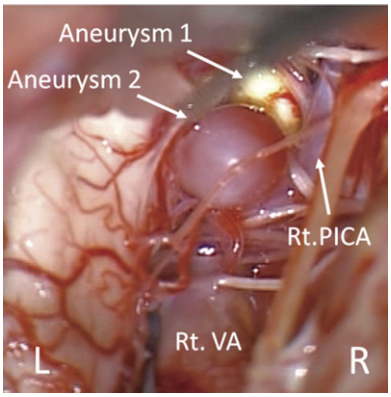

Figure 3. Intraoperative photograph showing two growing aneurysms originating in the right PICA. The proximal aneurysm (Aneurysm 1) had a yellowish wall with atherosclerosis, whereas the distal one (Aneurysm 2) had a reddish and rather thin wall. PICA, posterior inferior cerebellar artery; Rt., right; VA, vertebral artery.

Vessel and Aneurysm Modeling

Digital angiography was performed by standard transfemoral catheterization of the right VA, and digital imaging was performed using a biplanar unit (Innova 3131; General Electric Healthcare Japan, Tokyo, Japan). These images were obtained during a 6-second injection of a contrast agent and a 200-degree rotation with imaging at 30 frames per second for a total of 8 seconds. The corresponding 150 projection images were reconstructed into a 3D data set consisting of 512 × 512 × 512 isotropic voxels covering a field of view of 20 mm in all three directions. The images were reconstructed using a dedicated workstation.

The data set was exported to a personal computer to form 3D isosurfaces of the aneurysm using imaging software (Avizo 6.2; Visualization Science Group, Merignac, France). To provide consistent geometries from the data at three different time points, we identified on the baseline data set a reference vessel segment—the right VA—that remained unchanged over time. The mean value of the right VA was calculated, and one-half of the mean value was selected as the first threshold for defining intraluminal vessel volume. The segmented luminal surface was then displayed on native axial, coronal, and sagittal slices of 3D angiographic images until the displayed luminal surface visually matched the luminal boundary of all regions of interest. To provide a consistent threshold from baseline to follow-ups,

the three geometries were semiautomatically coregistered, and thresholds were adjusted to maintain the same reference diameter in subsequent segmentations.

The entire model of the aneurysm complex, including both PICA aneurysms, was created using commercial software (Magics RP 13.1; Materialise, Leuven, Belgium). Care was taken to ensure proper length of the parent artery (VA). The volumetric grid, composed of tetrahedral elements, was generated using meshing software (Gambit 2.4; ANSYS Inc., Lebanon, New Hampshire, USA) with a resolution of 0.1 mm, resulting in approximately 1.5 million element meshes.

Quantitative MR Velocimetry

Quantitative MR velocimetry was performed on this patient using a 3-Tesla MR image scanner (Signa HDxt 3.0T: General Electric Healthcare Japan) just before the last angiography. The protocol entails performing a standard axial 2D time-of-flight MR angiography of the cranial vasculature to select a slice orientation for the arterial blood flow measurements. The optimal perpendicular scan plane was determined using the acquired time of flight images. The coordinates obtained specify the position of an oblique fast 2D phase-contrast sequence, which was then performed based on these coordinates using a peripheral gated 2D phase-contrast sequence with the following imaging parameters: repetition time, 25; echo time, 5.4; number of excitations, 1; field of view, 160 × 160 mm; matrix, 512 × 512; voxel size, 0.3 × 0.3 mm; velocity encoding, 100 and 50 cm/s for the VA and PICA, respectively; imaging time, approximately 5 minutes; transaxial direction; peripheral gated with electrocardiography, 30 phases. The phase-contrast images were transferred to the workstation for flow quantification using dedicated software (CV flow; General Electric Healthcare Japan). A region of interest was semiautomatically placed on the phase-contrast images over one cardiac cycle. The velocities at all of the pixels inside the vessel border were integrated to calculate the flow in milliliters per minute. The quantitative waveform over one cardiac cycle was then drawn using these flow rates.

The flow rates were 83.3 and 12.2 mL/min in the right VA and right PICA, respectively. The waveform for the right VA was used as the inlet condition in numerical simulations, and the calculated fractional flow rates were specified for two outlet boundaries: 0.15 for the right PICA and 0.85 for the right VA.

CFD Simulations

Following the conventions for CFD in large vessels (3), blood was treated as an incompressible Newtonian fluid; vessel walls were assumed rigid, and no-slip boundary conditions were applied at the walls. A finite-volume package, Fluent (ANSYS Inc), was used to solve the governing equations: 3D unsteady Navier-Stokes equations and the equation of continuity. Patient-specific pulsatile flow conditions, derived from the MR velocimetry at the second follow-up, were prescribed at the inlet boundary (the right VA) of the three models. It was assumed that the waveform does not change appreciably over time. The diffusion fluxes in the direction normal to the inlet plane were assumed to be zero, and normal gradients were neglected. For the two outlet boundaries, we specified the fractional flow rate through each outlet calculated from the results of the MR velocimetry. A total of three cardiac cycles were computed using 100 time-steps per cycle; the results for the third cycle are presented.

Data Analysis

To visualize flow patterns, 3D streamlines of intra-aneurysm flow at peak systole and end diastole exiting the PICA were plotted in the model at each time point (baseline, first follow-up, and second follow-up) using commercial software (ANSYS CFD; ANSYS Inc).

WSS refers to the tangential frictional stress caused by the action of blood flow on the vessel wall. For pulsatile flow, the time-averaged WSS was calculated by integrating WSS magnitude over a cardiac cycle for each tetrahedral element (9):

$$WSS = \frac{1}{T}\int_0^T \left|\vec{\tau}_w\right| dt,$$

where $\vec{\tau}$ is the instantaneous WSS vector and T is the duration of the cycle. Because low WSS has been associated with aneurysm growth and rupture (18, 19, 22), we calculated WSS for the entire model at each time point.

To describe the temporal disturbance of intra-aneurysm flow, oscillatory shear index (OSI), a dimensionless measure of directional changes in WSS, was calculated using the formula reported by He and Ku (7):

$$OSI = \frac{1}{2}\left[1 - \frac{\left|\int_0^T \vec{\tau}_w dt\right|}{\int_0^T \left|\vec{\tau}_w\right| dt}\right].$$

Note that $0 \leq OSI < 0.5$, with 0 being completely unidirectional shear and 0.5 being completely oscillatory. Because high OSI has been shown to be significant for ruptured aneurysms (22), we suspected that it might also be related to aneurysm growth. Therefore, we calculated the OSI for the entire model at each time point.

RESULTS

Figure 4A shows reconstructed 3D models of the PICA aneurysm complex from the three angiographs: the baseline and two follow-ups. To clearly visualize the regions of aneurysm growth, we overlapped three models by aligning the VA to achieve accurate matching, because this parent artery experienced no change over the observation period (**Figure 4B**). Clearly, the proximal aneurysm (Aneurysm 1) grew slightly on the superior side, whereas the distal aneurysm (Aneurysm 2) showed enlargement of the whole aneurysm body. Aneurysm 1, which was complex shaped with four blebs, grew in the region of the small bleb at the top, whereas the round-shaped Aneurysm 2 showed drastic enlargement of the whole sac. The extended tip at the bottom of Aneurysm 2 observed at the first follow-up suggests that its growth started from the bottom.

Figure 5 shows snapshots of the flow field (3D streamlines) captured at peak systole (A) and diastole (B). Note that the growing region of Aneurysm 1 experienced high-velocity flow. The inlet velocity waveform measured by MR velocimetry is also given.

Figure 6 shows the distribution of WSS and OSI in two views. Although **Figure 6A** presents the lateral view consistent with other figures presented above, the growing region in Aneurysm 1 cannot be examined in detail. To observe the growing region of Aneurysm 1 *en face*, we changed the viewing angle and plotted the results in **Figure 6B**.

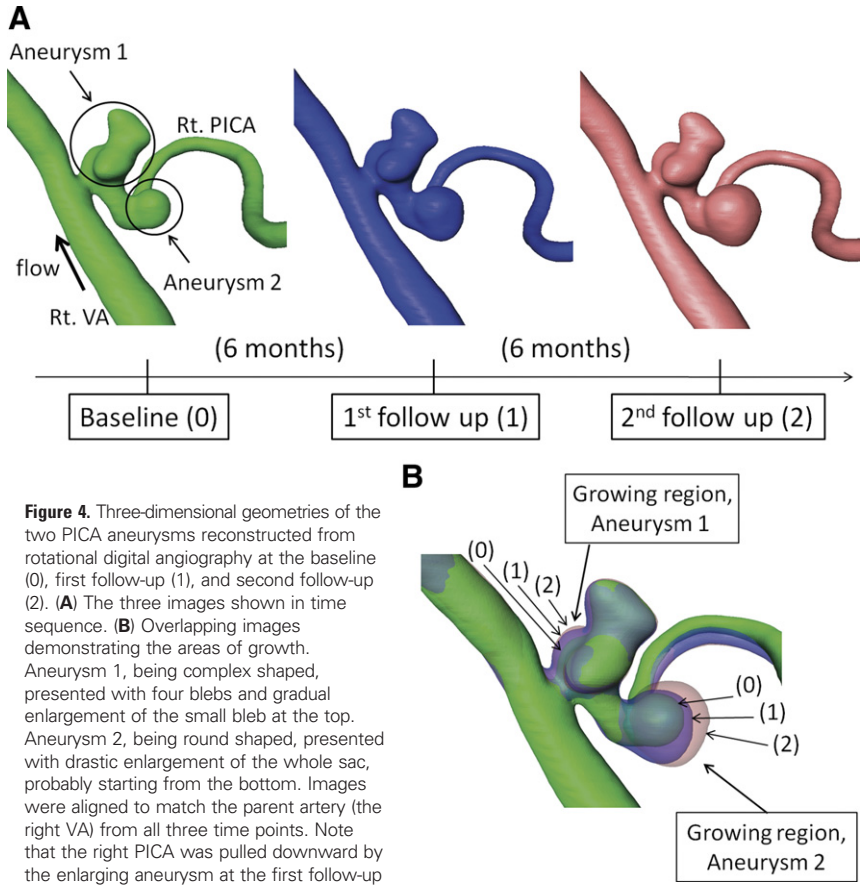

Figure 4. Three-dimensional geometries of the two PICA aneurysms reconstructed from rotational digital angiography at the baseline (0), first follow-up (1), and second follow-up (2). (**A**) The three images shown in time sequence. (**B**) Overlapping images demonstrating the areas of growth. Aneurysm 1, being complex shaped, presented with four blebs and gradual enlargement of the small bleb at the top. Aneurysm 2, being round shaped, presented with drastic enlargement of the whole sac, probably starting from the bottom. Images were aligned to match the parent artery (the right VA) from all three time points. Note that the right PICA was pulled downward by the enlarging aneurysm at the first follow-up and remained in that position at the second follow-up. PICA, posterior inferior cerebellar artery; Rt., right; VA, vertebral artery.

From **Figures 5** and **6**, it is evident that the growing area in Aneurysm 1 (a mild bleb on the top) was located near the inflow zone and therefore experienced high-velocity flow near the wall, as shown by the colored streamlines in **Figure 5**. This growing region was subjected to physiological levels of WSS (0.45–1.20 Pa) (10, 18), much higher than the WSS (~0.30 Pa) experienced by the more protruded blebs on Aneurysm 1. As this bleb enlarged, its WSS decreased. The OSI in the growing bleb was initially lower than that in the other blebs but increased with time.

Aneurysm 2, on the other hand, experienced low intra-aneurysm flow in its growing sac. It started with a rather low WSS (0.02–0.45 Pa) and a high OSI (~0.29) at the baseline; as the whole sac enlarged, the WSS sequentially decreased and the OSI sequentially increased. Time-resolved visualization (not shown) revealed that the flow field in Aneurysm 2 was unstable, with the flow divisions and vortex structures moving around during the cardiac cycle (12). The intra-aneurysm flow during the cardiac cycle became more and more unstable as the aneurysm sac enlarged, which is consistent with the increase in the OSI.

DISCUSSION

The purpose of this study was to determine whether there were differences in the hemodynamics of two adjacent aneurysms that presented different morphologic and vascular characteristics and were growing in different ways. One aneurysm (Aneurysm 1), which was multilobular in shape, already had three prominent protrusions (lobes) with an atherosclerotic wall. During the examination period, it was seen to grow on a fourth bleb. The other aneurysm (Aneurysm 2) was reddish, thin walled, and round. It grew rapidly by enlargement of the whole sac during the time interval before the next follow-up. Flow simulations revealed that the growing bleb of the multilobular aneurysm was located near the inflow zone and demonstrated high-velocity flow and physiological levels of WSS. In contrast, the large round aneurysm showed low intra-aneurysm flow, low WSS levels, and unstable flow patterns (higher OSI) in the dome. We speculate that the differences in the hemodynamic, morphological, and vascular characteristics of these two aneurysms indicate different mechanisms for their growth.

Regarding the partial growth of Aneurysm 1, high WSS has been postulated to account for aneurysm progression from the distal neck, where flow is impeded (6, 8). Meng et al. have shown that in animal models, high flow impact leading to high WSS and steep gradients of stress can cause destructive remodeling of the wall and aneurysm initiation (12, 14, 15). Cebral et al. showed that high flow impact might be an indicator of bleb formation and that most blebs progress to low WSS states after the blebs are formed (4). Shojima et al. speculated that such flow impact produces a steep shear gradient near the impact zone and accelerates the low shear-mediated process on the aneurysm wall (18). These underlying mechanisms might explain the growth of Aneurysm 1 and suggest that the growing region of Aneurysm 1 was in the process of developing a bleb like the other three blebs on this aneurysm. The intraoperative view of Aneurysm 1 at the end of examination period did not expose the growing region; therefore, we do not know if the wall of the growing region was yellowish with atherosclerotic plaque like the other part of this aneurysm or if it was reddish and thin walled like Aneurysm 2.

The growth of Aneurysm 2, in a low shear stress environment, may be consistent with observations by Boussel et al. (1). In their excellent longitudinal study, seven growing aneurysms were followed using 1.5-T MR angiography and patient-specific CFD. They found that aneurysm growth occurred in the wall exposed to abnormally low WSS (1). Our simulations (with higher resolution geometries derived from 3D rotational angiography) produced similar results, showing association of low WSS with aneurysm growth. In addition to low WSS, we suggest

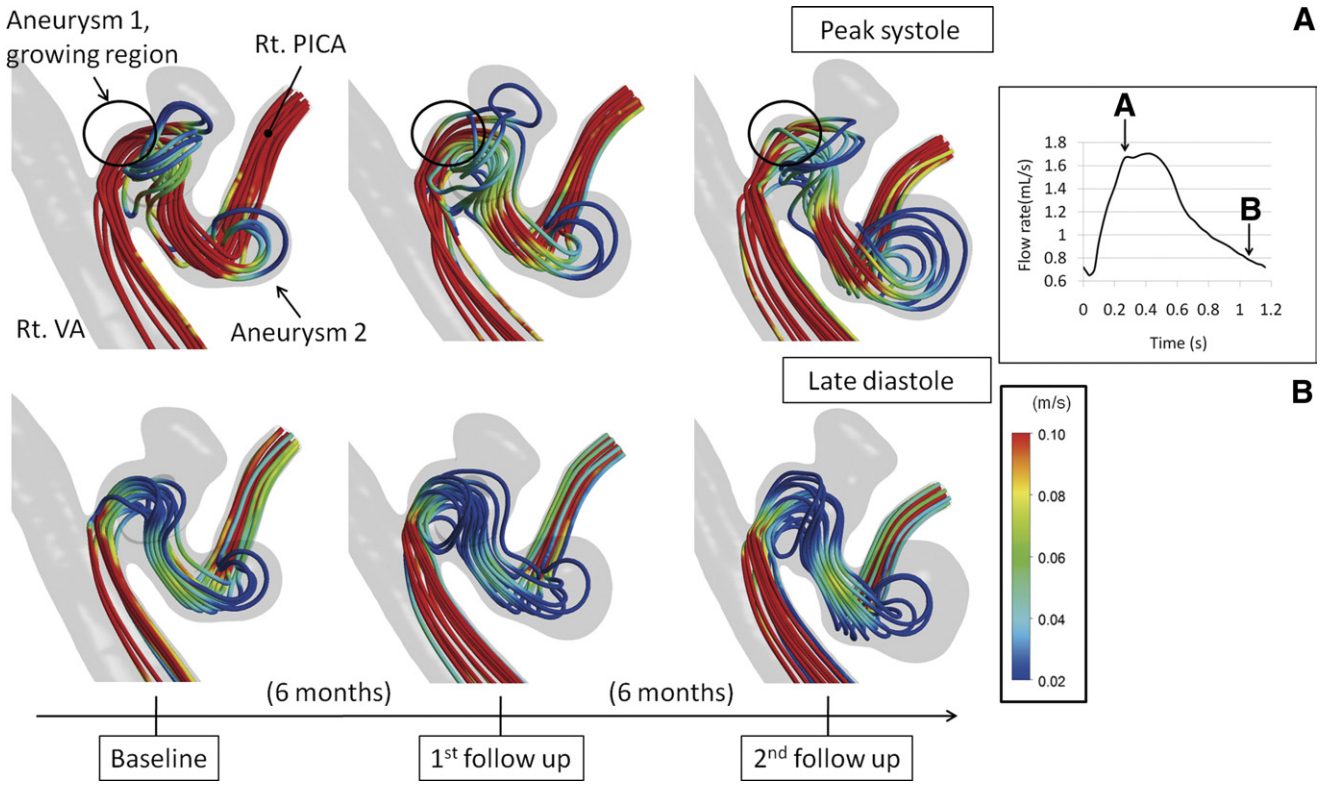

Figure 5. Snapshots of flow field (3D streamlines) captured at peak systole (**A**) and late diastole (**B**) as indicated on the inlet velocity waveform measured at the right vertebral artery by MR velocimetry during the second follow-up. The same waveform was used to run all three simulations. Note that the growing region of Aneurysm 1 experienced high flow near the entrance. PICA, posterior inferior cerebellar artery; Rt., right; 3D, three-dimensional; VA, vertebral artery.

that such aneurysm growth is associated with a high OSI, which indicates unstable, disturbed flow with significant directional change of WSS during the cardiac cycle. Xiang et al. found that WSS and the OSI are the significant hemodynamic factors that determine aneurysm rupture (22).

Our findings support those of Boussel et al. (1), suggesting a correlation between low aneurysmal flow hemodynamics and aneurysm growth. Our study did not indicate a causal relationship between the two, although such a relationship is entirely possible. Blood vessels can remodel in response to an abnormal hemodynamic environment (10). Aneurysm enlargement could be driven by biological processes mediated by unfavorable hemodynamic conditions such as low and oscillatory fluid shear stress, which have been shown to activate atherogenic and proinflammatory signaling pathways in endothelial cells (5, 11, 17). Activation of such inflammatory pathways might cause degradation of the aneurysm wall and growth of the aneurysm.

Our current study, based on patient-specific geometries, suggests that aneurysm growth is associated with a decrease in WSS and an increase in the OSI. Although it is not clear whether low WSS and a high OSI influence aneurysm growth, the reverse is almost certainly true: aneurysm geometry changes will result in changes of intra-aneurysm flow dynamics because geometry determines the flow. As demonstrated in numerical experiments by Tremmel et al. (21), aneurysm enlargement is followed by a decreased WSS on the aneurysm wall and often by an increased flow instability (the flow splits into multiple vortices that move around). Increased flow instability is accompanied by increased directional changes of fluid shear stress on the aneurysm wall, thus increasing the OSI.

The unanswered but highly intriguing question is whether certain hemodynamic factors, such as the high flow in the inflow zone of Aneurysm 1 and the disturbed flow in the dome of Aneurysm 2, are responsible for aneurysm growth. Further clinical studies are required to ascertain the significance of the relationship between hemodynamics and aneurysm history. In vivo studies are required to clarify the mechanobiological effects of hemodynamic factors on the aneurysm wall. Such an understanding could lead to exciting opportunities for predicting aneurysm growth by image-based CFD.

Our CFD simulations include typical simplifications made in model generation and boundary conditions (20). Several biological properties such as the viscoelasticity of the vessel wall and the non-Newtonian property of the blood are neglected for technical reasons. For the inlet condition, we used a pulsatile waveform obtained on this patient before the third angiography for all three simulations. It should be pointed out that this is an improvement over what has been typically done in CFD, where a non-patient-specific waveform is used as the inlet condition (2). We believe that despite these simplifications, our CFD analysis has captured the main hemodynamic features of growing aneurysms. The region of aneu-

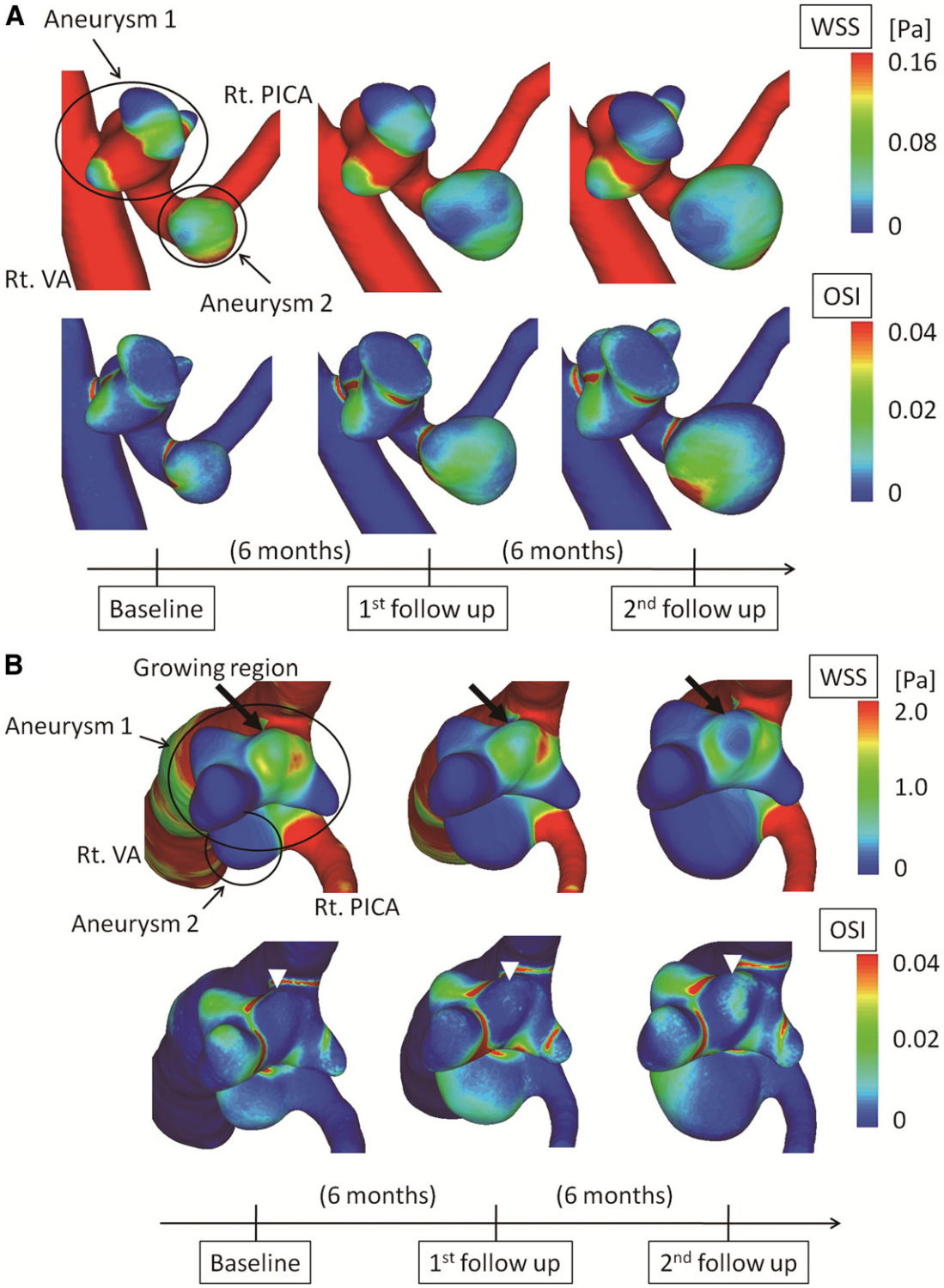

Figure 6. Distribution of time-averaged wall shear stress (WSS) and oscillatory shear index (OSI) in two views: (**A**) Lateral view consistent with **Figures 2–5**; (**B**) En face view of the growing area in Aneurysm 1 (blood in VA comes towards the reader). As evident from **B**, the growing region of Aneurysm 1 experienced higher WSS and lower OSI than the more protruded blebs; however, as this bleb enlarged, the WSS is seen to decrease (*black arrow*) and OSI to slightly increase (*white arrowhead*) with time. Aneurysm 2, on the other hand had rather low WSS (seen from both **A** and **B**) and high OSI (seen from **A**) to start with, and as the whole sack enlarged, the WSS continued to decrease and OSI continued to increase. Note that the scale of WSS in **A** is smaller than that in **B**. PICA, posterior inferior cerebellar artery; Rt., right; VA, vertebral artery.

rysm growth could experience either high WSS at the inflow zone or low WSS and a high OSI in the aneurysm sac.

CONCLUSIONS

We have shown two growing aneurysms with different hemodynamic characteristics and growing patterns: a proximal multilobular aneurysm was growing a bleb near the inflow zone with high local velocity and physiological levels of WSS, whereas a distal rounded aneurysm was growing the entire sac featuring low and unstable intra-aneurysmal flow, with low WSS and higher OSI. Thus, growing aneurysms may have heterogeneous hemodynamic, morphologic, and vascular characteristics associated with different mechanistic pathways.

REFERENCES

1. Boussel L, Rayz V, McCulloch C, Martin A, Acevedo-Bolton G, Lawton M, Higashida R, Smith WS, Young WL, Saloner D: Aneurysm growth occurs at region of low wall shear stress: patient-specific correlation of hemodynamics and growth in a longitudinal study. Stroke 39:2997-3002, 2008.

2. Cebral JR, Mut F, Weir J, Putman CM: Association of hemodynamic characteristics and cerebral aneurysm rupture. AJNR Am J Neuroradiol 32:264-270, 2011.

3. Cebral JR, Mut F, Weir J, Putman C: Quantitative characterization of the hemodynamic environment in ruptured and unruptured brain aneurysms. AJNR Am J Neuroradiol 32:145-151, 2011.

4. Cebral JR, Sheridan M, Putman CM: Hemodynamics and bleb formation in intracranial aneurysms. AJNR Am J Neuroradiol 31:304-310, 2010.

5. Chiu JJ, Chen CN, Lee PL, Yang CT, Chuang HS, Chien S, Usami S: Analysis of the effect of disturbed flow on monocytic adhesion to endothelial cells. J Biomech 36:1883-1895, 2003.

6. Hashimoto T, Meng H, Young WL: Intracranial aneurysms: links among inflammation, hemodynamics and vascular remodeling. Neurol Res 28:372-380, 2006.

7. He X, Ku DN: Pulsatile flow in the human left coronary artery bifurcation: average conditions. J Biomech Eng 118:74-82, 1996.

8. Hoi Y, Meng H, Woodward SH, Bendok BR, Hanel RA, Guterman LR, Hopkins LN: Effects of arterial geometry on aneurysm growth: three-dimensional computational fluid dynamics study. J Neurosurg 101:676-681, 2004.

9. Lee SW, Antiga L, Steinman DA: Correlations among indicators of disturbed flow at the normal carotid bifurcation. J Biomech Eng 131:061013, 2009.

10. Malek AM, Alper SL, Izumo S: Hemodynamic shear stress and its role in atherosclerosis. J Am Med Assoc 282:2035-2042, 1999.

11. Malek AM, Higashida RT, Halbach VV, Phatouros CC, Meyers PM, Dowd CF: Tandem intracranial stent deployment for treatment of an iatrogenic, flow-limiting, basilar artery dissection: technical case report. Neurosurgery 45:919-924, 1999.

12. Meng H, Metaxa E, Gao L, Liaw N, Natarajan SK, Swartz DD, Siddiqui AH, Kolega J, Mocco J: Progressive aneurysm development following hemodynamic insult. J Neurosurg 114:1095-1103, 2011.

13. Meng H, Swartz DD, Wang Z, Hoi Y, Kolega J, Metaxa EM, Szymanski MP, Yamamoto J, Sauvageau E, Levy EI: A model system for mapping vascular responses to complex hemodynamics at arterial bifurcations in vivo. Neurosurgery 59:1094-1100, 2006.

14. Meng H, Wang Z, Hoi Y, Gao L, Metaxa E, Swartz DD, Kolega J: Complex hemodynamics at the apex of an arterial bifurcation induces vascular remodeling resembling cerebral aneurysm initiation. Stroke 38:1924-1931, 2007.

15. Metaxa E, Tremmel M, Natarajan SK, Xiang J, Paluch RA, Mandelbaum M, Siddiqui AH, Kolega J, Mocco J, Meng H: Characterization of critical hemodynamics contributing to aneurysmal remodeling at the basilar terminus in a rabbit model. Stroke 41:1774-1782, 2010.

16. Nixon AM, Gunel M, Sumpio BE: The critical role of hemodynamics in the development of cerebral vascular disease. J Neurosurg 112:1240-1253, 2010.

17. Passerini AG, Polacek DC, Shi C, Francesco NM, Manduchi E, Grant GR, Pritchard WF, Powell S, Chang GY, Stoeckert CJ Jr, Davies PF: Coexisting proinflammatory and antioxidative endothelial transcription profiles in a disturbed flow region of the adult porcine aorta. Proc Natl Acad Sci U S A 101:2482-2487, 2004.

18. Shojima M, Nemoto S, Morita A, Oshima M, Watanabe E, Saito N: Role of shear stress in the blister formation of cerebral aneurysms. Neurosurgery 67:1268-1274, 2010.

19. Shojima M, Oshima M, Takagi K, Torii R, Hayakawa M, Katada K, Morita A, Kirino T: Magnitude and role of wall shear stress on cerebral aneurysm: computational fluid dynamic study of 20 middle cerebral artery aneurysms. Stroke 35:2500-2505, 2004.

20. Steinman DA, Taylor CA: Flow imaging and computing: large artery hemodynamics. Ann Biomed Eng 33:1704-1709, 2005.

21. Tremmel M, Dhar S, Levy EI, Mocco J, Meng H: Influence of intracranial aneurysm-to-parent vessel size ratio on hemodynamics and implication for rupture: results from a virtual experimental study. Neurosurgery 64:622-630, 2009.

22. Xiang J, Natarajan SK, Tremmel M, Ma D, Mocco J, Hopkins LN, Siddiqui AH, Levy EI, Meng H: Hemodynamic-morphologic discriminants for intracranial aneurysm rupture. Stroke 42:144-152, 2011.

Conflict of interest statement: The authors declare that the research was conducted in the absence of any commercial or financial relationships that could be construed as a potential conflict of interest. H. M. receives grants from the National Institutes of Health.

Received 04 July 2011; accepted 06 September 2011; published online 01 November 2011

Citation: World Neurosurg. (2012) 78, 5:462-468.
DOI: 10.1016/j.wneu.2011.09.023

Journal homepage: ***www.WORLDNEUROSURGERY.org***

Available online: ***www.sciencedirect.com***